Egypt. J. Chem. **Vol. 65**, No. SI:13B pp. 557 - 569 (2022)

Egyptian Journal of Chemistry

http://ejchem.journals.ekb.eg/

Facile Green Synthesis of ZnO Supported on Exfoliated Graphite for Photocatalytic Degradation of Dye under UV and Visible-Light Irradiation

Enas Amdeha[a], *, Marwa S. Salem[b]

[a]*Egyptian Petroleum Research Institute (EPRI), Nasr City, Cairo, 11727, Egypt.*

[b]*Botany and Microbiology Dept., Faculty of Science Al-Azhar University, Nasr City, Cairo, Egypt.*

Abstract

Visible light-responsive photocatalysis is a green and efficient wastewater treatment technique, and carbon materials-based semiconductors have demonstrated excellent performance in this area. In this work, zinc oxide nanoparticles (ZnO NPs) are synthesized via a simple, economic and green method using *Streptomyces* microbial extract as non-toxic reducing and capping agent. The prepared ZnO is supported on the exfoliated graphite (ZnO/EG) by a simple mixing method. Various techniques including XRD, FTIR, DLS, Zeta, BET, TEM and optical properties of the prepared photocatalysts were elucidated. The results reveal that the ZnO particles are well dispersed on the EG in the ZnO/EG sample. Also, diffuse reflectance spectroscopy revealed that the ZnO/EG nanocomposite possesses an increased light absorption toward the visible light region, as a result of the presence of the EG. The photocatalytic performance of the prepared photocatalysts was discussed using Malachite Green (MG) dye under both UV and visible light. The effect of dye concentration, photocatalyst dose, pH and different scavengers was studied. The activity of the ZnO/EG (94.06 %, rate, k = 0.0184 min^{-1}) is enhanced under visible light rather than ZnO alone (50.05 %, rate, k = 0.0030 min^{-1}), which will be a promising and competing candidate for wastewater treatment.

Keywords: Exfoliated graphite; Malachite green dye; Photocatalysis; Streptomyces; Visible light; ZnO

1. Introduction

Water is a very important wealth for a living being. Though water covers over 71 per cent of the earth's surface, only about 3.5 per cent of that is freshwater, with the remainder being salty [1]. Moreover, high consumption, population growth, industrialization, climate change and environmental pollution cause water scarcity [2]. According to the World Health Organization (WHO), over 80 per cent of the world's wastewater remains untreated. Moreover, more than one billion people are searching for a clean supply of drinking water [3]. Because of the acute need for drinking water, many populations are in danger of consuming polluted water supplies, which can lead to disease and economic disruption. Industrial effluents and household discharges are the two main sources of wastewater. Textile industries release approximately more than 100,000 t of dyes per year into water bodies. The spillage of these hazardous effluents in the environment causes severe negative effects on human and animal health as well as on aquatic life [4,5]. Among the various organic dyes, Malachite green (MG) dye has gotten a lot of attention due to its usage as a fungicide and disinfectant in the fish farming industry as well as in the textile industry. It is critical to remove MG from wastewater because of its teratogenic, carcinogenic, and mutagenic effects in humans [2]. These coloured effluents are recognized as toxic wastes by the Environmental Protection Agency (EPA) even at minor concentrations. To avoid these harmful effects, these pollutants have to be removed or reduced to acceptable levels before discharging into water bodies [6,7].

For wastewater treatment, several processes were used, including solvent extraction, filtration, chemical precipitation, adsorption, ion exchange, and reverse osmosis [8,9]. However, these processes do not achieve total pollutants degradation; rather, they transfer pollutants from water to other media, resulting in other pollution. Advanced oxidation processes (AOPs) are effective in the treatment of wastewater as they rely on the formation of potent reactive species that can completely degrade organic water contaminants [10–13]. Biosynthesis of nanoparticles is a method of synthesizing nanoparticles utilizing microbial and plants extracts. This method is eco-friendly, cost-effective, biocompatible, safe, and has environmental benefits. Plants, fungi, bacteria, algae,

*Corresponding author e-mail: enas_amdeha@yahoo.com.

Receive Date: 19 April 2022, Revise Date: 11 May 2022, Accept Date: 18 May 2022

DOI: 10.21608/EJCHEM.2022.130532.5931

and other organisms are all used in green synthesis. They enable the manufacture of NPs on a large scale without any impurities. Biomimetic NPs have higher catalytic activity and need fewer expensive and harmful ingredients to produce. These natural strains and plant extracts produce phytochemicals that function as a reducing agent as well as a capping or stabilizing agent [14].

Among the semiconductors, ZnO has gained great consideration due to its extraordinary properties [15]. However, because of the large bandgap of ZnO, it can only be activated by UV light. Also, the photogenerated e^-/h^+ pairs have a short lifetime, and the application of ZnO as a photocatalyst is limited. To solve these issues, it is important to build ZnO-based photocatalysts with high photoactivity under visible light with enhanced charge separation. The aim of working under visible light is to reduce energy consumption and the total cost of the photodegradation process. As visible light accounts for > 43 % of the solar spectrum, if the photocatalyst is visible light-responsive, the photocatalytic process can be done under renewable costless sunlight irradiation. Herein the applied technique to widen the light absorption range of ZnO to the visible light region and to enhance the charge separation is the supporting of ZnO on the exfoliated graphite as the latter possesses a high absorption range.

Carburet (United States) discovered exfoliated graphite (EG), a carbon substance with a loose porous structure and low density, in 1968. Microwave or high-temperature treatment of graphite produced by chemical or physical means is the most common method of obtaining EG [16]. This approach produces materials with significant expansion volumes at a reasonable cost [17]. Exfoliated graphite was employed by Carvallho et al. [18] and Van Pham et al. [19] to remove the blue textile and Congo red dyes, respectively. Nevertheless, the photodegradation of MG using bio-based ZnO/EG is not yet studied.

To the best of our knowledge, supporting *Streptomyces*-based ZnO on the exfoliated graphite as a facile green synthesized photocatalyst for Malachite Green photodegradation under both UV and visible light irradiation is not studied yet. In this work, facile methods were applied to prepare exfoliated graphite, bio-based ZnO using bacterial extract as a green approach and bio-based ZnO supported on the exfoliated graphite (ZnO/EG) composite by a simple mixing method. The synthesized photocatalysts were characterized via different techniques and their photodegradation performance under both UV and visible light irradiation was examined using MG dye as a model pollutant. The effect of different parameters on the photodegradation process was elucidated. Also, the effect of the active species was performed via scavenger test.

2. Experimental

2.1. Materials

Graphite fine powder (98%; 60 mesh; LOBA Chemie), Zinc nitrate ($Zn(NO_3)_2.6H_2O$; 96%; LOBA Chemie), Malachite green (MG) dye ($C_{23}H_{25}N_2Cl$; MW = 364.92 g; λ_{max} = 615 nm; Fluka), distilled water.

2.2. Synthesis of Exfoliated Graphite (EG)

Exfoliated graphite (EG) was prepared by placing the graphite powder in an electric furnace at 600 ºC for four hours [7].

2.3. Preparation of microbial extract

Streptomyces fradiae had previously been isolated from a polluted location in Egypt from Helwan City. 16S rRNA sequencing was used to identify the isolate, which demonstrated a high level of similarity (95%) with *S. fradiae* strain HBUM 174185 (Gen Bank accession number FJ486352.1) [20]. For the green synthesis of the ZnO nanoparticles, the *actinomycete* strain was grown in a starch nitrate broth medium for 7 days at 30 ºC and 150 rpm. The culture was then centrifuged at 10 000 rpm for ten minutes, and the supernatant was collected [21].

2.4. Synthesis of Zinc Oxide nanoparticles (ZnO NPs)

A facile and environmentally benign process was used to synthesize ZnO NPs. Two grams of $Zn(NO_3)_2.6H_2O$ were dissolved in 100 ml of recently made *Streptomyces fradiae* extract solution and then rapidly agitated for one hour at 60 ºC. The obtained white precipitate was filtered and dried at 80 ºC overnight. Finally, the product was calcined at 400 ºC for two hours.

2.5. Synthesis of binary nanocomposite ZnO/EG

The binary nanocomposite; 20% ZnO/EG; was prepared by a facile mixing method, in which the prepared ZnO and EG were mixed vigorously by mortar.

2.6. Characterization techniques

X-ray diffractometer (XRD, Shimadzu XD-1, Japan), Fourier Transform Infrared (FTIR, Nicolet Is-10 model, USA), Dynamic light scattering (DLS, Malvern-ZS, Ltd., UK, nano series), Nitrogen-adsorption-desorption isotherms (BET, a NOVA-3200, USA), Transmission electron microscope (TEM, JEM-1230, JEOL, Japan), Diffuse reflectance spectroscopy (DRS, a JASCO, V–570, Japan) and photoluminescence (PL, JASCO, FP–6500, Japan).

2.7. Photodegradation of malachite green (MG)

The photocatalytic performance of the prepared photocatalysts was assessed by the degradation of the aqueous solutions of MG dye under both UV and visible light irradiation. To run the experiment, (20 mg) of each sample was added to 100 ml of the (100 ppm, MG) solution in a batch reactor and left in dark for one hour with stirring to attain equilibrium. After that, the reaction was exposed to a UV (8W VILBER–LOURMAT; λ=254 nm) or visible light (100W–TUNGSTEN lamp; λ > 400 nm) for three hours. At a fixed time, interval, 4 ml of the suspension were withdrawn and centrifuged to remove the photocatalyst. The remaining dye concentration was measured using a UV-visible spectrophotometer (JENWAY–6505). Similar reactions were adopted for the parameters study e.g. dye concentration, photocatalyst dose, and pH. Also, the scavengers test was studied.

3. Results and Discussion

3.1. Characterization

XRD is a technique for determining the crystallinity of materials and inferring structural changes in the components involved in a reaction. **Fig. 1** shows the XRD patterns of the synthesized ZnO/EG binary nanocomposite and the single compounds (ZnO and EG). The synthesized ZnO nanoparticles **Fig. 1 (a),** exhibited the presence of the hexagonal Wurtzite structure (Card No. 04-007-5097) with an average crystallite size of 56.6 nm, confirming the successful usage of the biological extract as a facile green reducing agent for the ZnO synthesis in nano-scale. Consequently, exact diffraction peaks at 31.66º, 34.43º, and 36.12º are seen in the ZnO sample pattern, which correspond to the (1 0 0), (0 0 2), and (1 0 1) ZnO crystal planes, respectively, which are in accordance with those reported in the literature for ZnO [22,23]. For EG sample, **Fig. 1 (b)**, the pattern displays two main characteristic peaks at $2\theta_1$ = 26.4º (d_1 = 0.337 nm) and $2\theta_2$ = 54.49º (d_2 = 0.168 nm) which are in coincident with the graphitic carbon (Card No. 04-007-2076) confirming the successful fabrication of the EG. These peaks are assigned to the 0 0 2 and 0 0 4 planes of the exfoliated graphite, respectively [24]. A sharp peak at 26.4º confirmed the crystalline nature with an average crystalline size equal to 42.2 nm [25]. For the ZnO/EG sample, **Fig. 1 (c),** the 0 0 2 plane is observed at 2θ = 26.59 º. The slight shift in the 2θ value towards a larger angle after mixing the EG with the ZnO leads to a decrease in the d-spacing from 0.337 nm for EG to be 0.335 nm for ZnO/EG [26]. It is also interesting to note that the ZnO/EG nanocomposite pattern shows that the ZnO phase exists with the EG phase with a minor increment in the average crystalline size to be 59.5 nm, indicating that the ZnO is successfully supported on the EG [27].

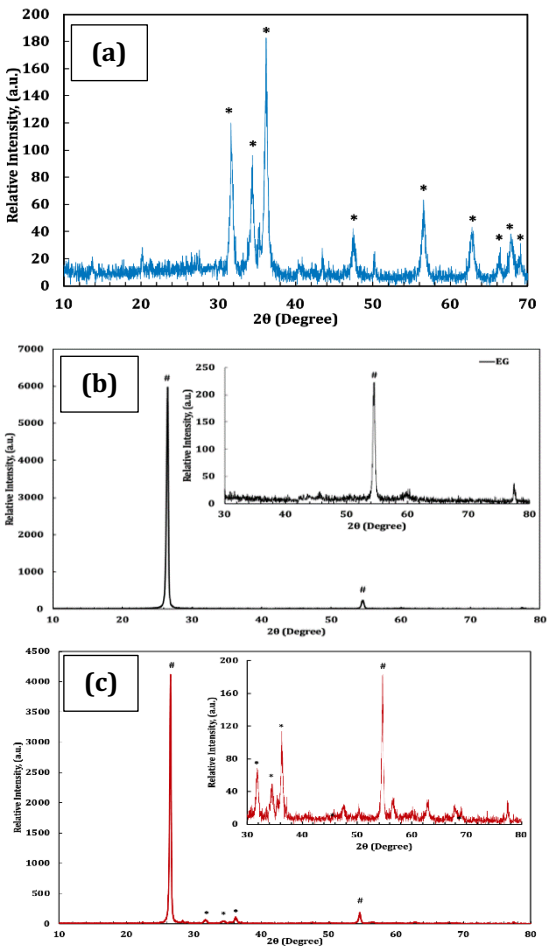

Fig. 1. XRD patterns of (a) ZnO, (b) EG and (c) ZnO/EG samples (* and # are for ZnO and EG peaks, respectively).

The chemical structure of the ZnO and EG as well as the binary nanocomposite ZnO/EG were characterized using FTIR, **Fig. 2**. The wideband at 3900–3650 cm^{-1} appears in the EG and ZnO/EG samples is due to the O–H stretching mode of OH–groups and adsorbed H_2O molecules that present in the samples' structure. Also, it is referred to the presence of the H–bonding of the OH–groups. Broad absorption peaks in the range of 3600–2950 cm^{-1}, are related to the deformation and vibration of H_2O molecules that are adsorbed on the samples' surfaces from the environment [28]. The peak around 1700 cm^{-1} is due to the existence of the COO–group [27]. The asymmetrical stretching vibration peak at 1630 cm^{-1} is related to the sp^2-hybridized C=C [17,29]. The peak at 1110 cm^{-1} is for the carbon fingerprint. This peak is also related to the symmetric and asymmetric C–O stretching vibration of –C–O–C– ring. The peak at 1056 cm^{-1} is related to the C–O and the C–C tensile vibrations [28]. The band between 900–670 cm^{-1} is related to the C–H bending mode [30]. The appeared peak at 465 cm^{-1} for both ZnO and ZnO/EG samples is for the hexagonal phase ZnO [31]. The peaks at 1540 cm^{-1} and 671 cm^{-1} in the EG sample are due to C–C bonds and the C=C

aromatic benzene ring, respectively, demonstrating that the graphite is of good quality and devoid of organic contamination [32,33]. For the ZnO spectrum, the peak at 3475 cm^{-1} (N–H stretch) was for the amine group as reported by Prakasham et al. (2014) [34] and Lakhsmi et al. (2015) [35]. Also, the peak at 1468 cm^{-1} is for C=O stretch and C–N stretch of amide in protein [36]. The fact that the amide groups of the proteins had a better ability to bind metal was corroborated by the FTIR spectrum of the ZnO nanoparticles, indicating that the proteins operate as a capping agent for stabilizing the nanoparticles [37]. From the mentioned XRD patterns, it is proved that ZnO/EG was successfully prepared. Moreover, the FTIR of the binary nanocomposite ZnO/EG exhibits functional groups of both ZnO and EG without any shifting. This confirms that the mixing process is a physical bonding process rather than a chemical reaction [38].

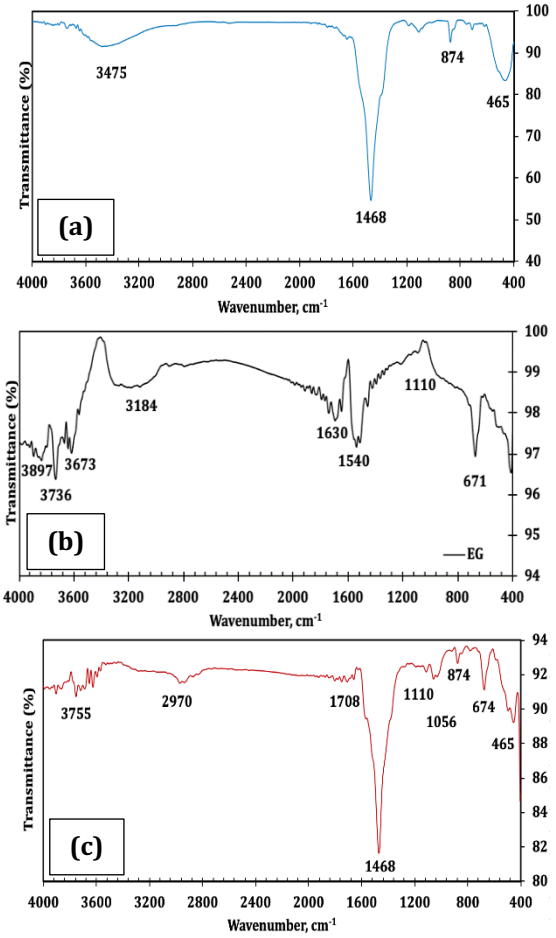

Fig. 2. FTIR spectra of (a) ZnO, (b) EG and (c) ZnO/EG samples.

To detect the particle size distribution based on the intensity in a suspended solution and also, determine the zeta potential, the DLS as one of the most familiar techniques are applied, **Fig. 3 (a – c)**. The particle sizes of the prepared ZnO, EG, ZnO/EG are 142 nm, 187 nm and 333 nm, respectively. The reason that there are differences in the particle sizes obtained by XRD and DLS, is that the DLS is not only associated with the particles' metallic core but also affected by the presence of the capping proteins and enzymes [39]. Thus, the particle sizes measured by DLS are commonly higher than those calculated by the Scherrer equation from XRD data.

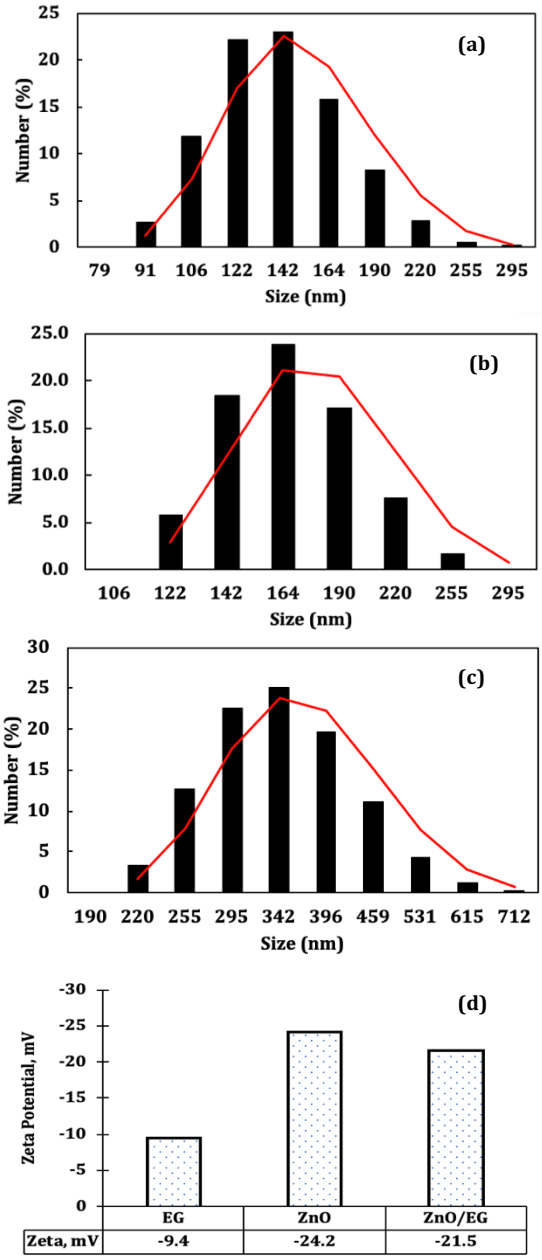

Fig. 3. Particle size distribution for (a) ZnO, (b) EG (c) ZnO/EG and (d) zeta potential.

The stability of the colloidal solution is related to the particles' surface charge which can be acquired by the Zeta potential analyzer. The high zeta potential values prevent particles aggregation. The zeta potential values for the prepared catalysts, **Fig. 3 (d)**, were -24.2 mV, -9.4 mV and -21.5 mV for ZnO, EG, and ZnO/EG, respectively. The support of the ZnO on the EG enhances the stability of the binary composite ZnO/EG as the zeta potential of the composite is enhanced from -9.4 mV for EG only to be -21.5 mV for the composite [40]. The catalysts which have high negative zeta potential, enhance the adsorption of the positively charged dyes, consequently, having a positive impact on the photocatalytic degradation of the dyes.

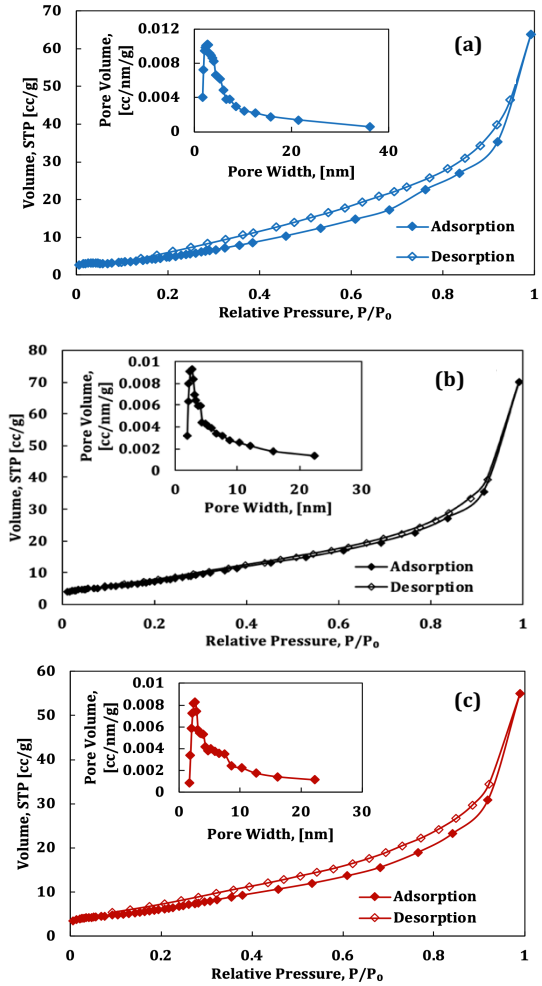

Fig. 4. Isotherms and the pore size distribution (insets) of the (a) ZnO, (b) EG and (c) ZnO/EG samples.

The specific surface area (SSA), isotherm and pore size distribution of the prepared ZnO, EG and ZnO/EG nanocomposite are studied by the N2 adsorption-desorption analyses using Brunauer-Emmett-Teller (BET) method, **Fig. 4**. The SSA and pore structure parameters are illustrated in **Table 1**.

Table 1

Specific surface area (SSA), pore volume (V_{pore}), and pore size (d_{pore}) of ZnO, EG and ZnO/EG samples.

Sample	SSA_{BET}, (m^2/g)	V_{pore}, (cm^3/g)	d_{pore}, (nm)
ZnO	23.42	0.099	16.8
EG	32.21	0.109	13.5
ZnO/EG	25.69	0.085	13.2

Generally, possessing a high specific surface area and good pore structure increases the pollutant adsorption rate and capacity which is promising from the photocatalysis point of view. The SSA of the ZnO/EG nanocomposite is slightly higher than that of the ZnO (23.42 m^2/g for ZnO and 25.69 m^2/g for ZnO/EG), this may be due to the support of the ZnO nanoparticles on the EG with a reasonable SSA (32.21 m^2/g for EG). The isotherms of ZnO, EG and ZnO/EG samples are of Type-IV with H3 hysteresis loops at P/P_o=0.2–0.95, which is characteristic of the mesoporous materials (e.g., carbon materials and industrial adsorbents). Meanwhile, the Barrett-Joyner-Halenda (BJH) method was used to examine the associated pore-size distribution curves, which confirmed that the ZnO, EG, and ZnO/EG exhibit the usual properties of mesoporous materials, with pore sizes primarily centered at 2.3–3.5 nm.

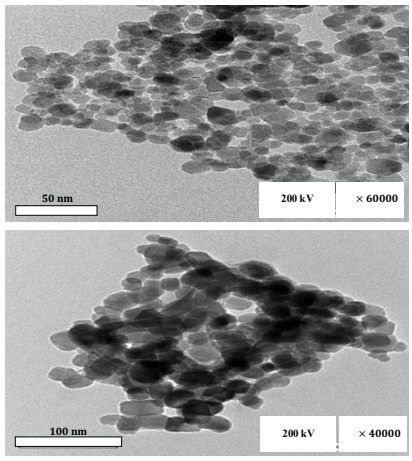

Fig. 5. TEM images of the ZnO/EG nanocomposite.

Transmission electron microscopy (TEM) has been employed to identify the morphology of the binary nanocomposite ZnO/EG synthesized by the green mixing method, **Fig. 5**. The TEM images reveal that the ZnO NPs with hexagonal shape are homogenously and greatly dispersed on the EG surface. The "well-dispersion" of the ZnO NPs over the EG in the whole matrix of the composite, confirms the good use of the mixing method to prepare the binary nanocomposite.

Additionally, there are some ZnO NPs with irregular shapes jointed to aggregate and regularly dispersed over the entire sample. These findings revealed that ZnO had been successfully established in EG.

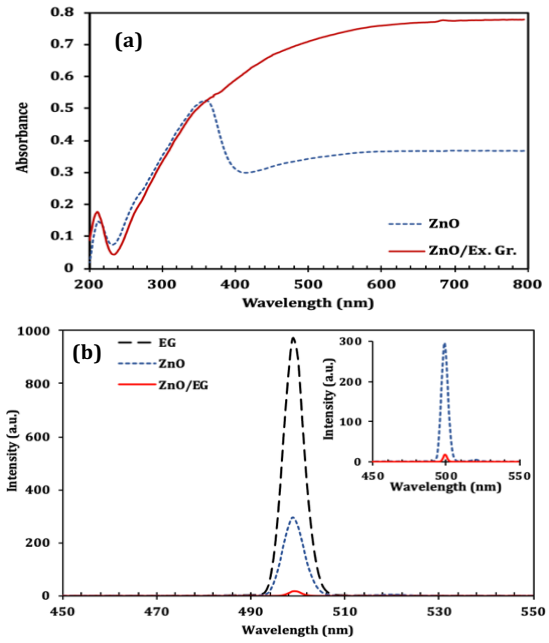

Fig. 6. UV–Vis absorption spectra (a) and PL (b) of the ZnO and ZnO/EG nanocomposite.

The UV-Visible absorption spectra and the photoluminescence spectra (PL) were engaged to explore the optical characteristics of the ZnO and ZnO/EG photocatalysts. It is remarkable to state that there is a meaningful shift in the absorption band for the binary nanocomposite ZnO/EG toward the visible light region. The hump for the ZnO NPs is obtained in the range of 320–380 nm, while the range for the ZnO/EG nanocomposite is extended to the visible region up to 800 nm. This highly visible response for the prepared nanocomposite is due to the presence of the EG as a support material for the ZnO NPs, **Fig. 6 (a)**.

Moreover, PL is an efficient method in the exploration of the optical properties of the semiconductors, involving electron-hole recombination rate. The emission peaks are caused by photo-induced e^- in the conduction band recombining with photo-induced h^+ in the valence band, resulting in excitons [41], **Fig. 6 (b)**. This peak may be due to the presence of defects in the sample structure which may exist as a result of the oxygen vacancies [42]. It is noted that the EG exhibited the highest PL intensity revealing that EG possesses the fastest e^-–h^+ recombination rate. While the binary nanocomposite ZnO/EG has the least e^-–h^+ recombination rate because photogenerated electrons are efficiently transferred from EG to ZnO [43]. Thus, the order of the recombination is EG>ZnO>ZnO/EG. This behaviour suggests the expected high photocatalytic performance of the prepared ZnO/EG toward the degradation of the organic pollutants under visible light illumination.

3.2. Photocatalytic Activity

The photocatalytic behaviour of the prepared EG, ZnO and the binary composite ZnO/EG was evaluated for the MG photodegradation under both UV and visible light irradiation, **Fig. 7** (a). It is critical to note that the detected colour loss of MG solution is due to a decrease in the absorbance of the MG chromophore's major absorption peak at 615 nm, which is caused by "n→π transitions" in the (C=N) group in the MG chromophore structure. As a result, the colour loss perceived is a spectrophotometrically determined decrease in absorbance at 615 nm [5]. The photolysis of the MG (with no catalyst) as a control experiment is negligible, demonstrating that the MG dye is steady under photolysis. The MG solution and the photocatalysts were stood in the dark for one hour to attain equilibrium. When conducting the adsorption for more three hours, there is no further obvious decrease in the MG concentration, indicating the first hour's achievement of the 'adsorption-desorption equilibrium'. Pure EG exhibits a high MG adsorption under dark (50 %) without any remarkable photodegradation under light irradiation. While ZnO exhibits a reasonable removal in dark due to the possessing of high negative zeta potential which enhances the electrostatic attraction between the negatively charged ZnO particles with the positively charged MG molecules [43].

Under visible light, the binary nanocomposite (ZnO/EG) exhibited the highest photocatalytic performance toward the MG degradation (94.06 %) as expected when compared to ZnO and EG (ZnO; 54.91 % and EG; 50 %), suggesting the synergetic effect of composing a binary nanocomposite of ZnO and EG. This may be owed to the aforementioned optical characteristics, as the supporting of the ZnO on the EG, is widen the light absorption range of the ZnO/EG toward the visible light region. Also, the presence of such carbon material as a highly conductive material, can strongly separate and transport the photogenerated e^-–h^+ carriers of the binary nanocomposite [44,45].

This result is important from the economic point of view, as by this method we can use about one-fifth of ZnO amount to degrading a high MG concentration under visible light irradiation by supporting ZnO on low-cost EG. This finding is consistent with the previous work [41], in which TiO_2 is supported on the activated carbon (AC) to enhance the Methylene Blue (MB) dye degradation under visible light irradiation. Generally, when using a carbon material as a support for a photocatalyst, the presence of such material

motivates the adsorption behaviour of the ZnO/EG binary composite photocatalyst for example.

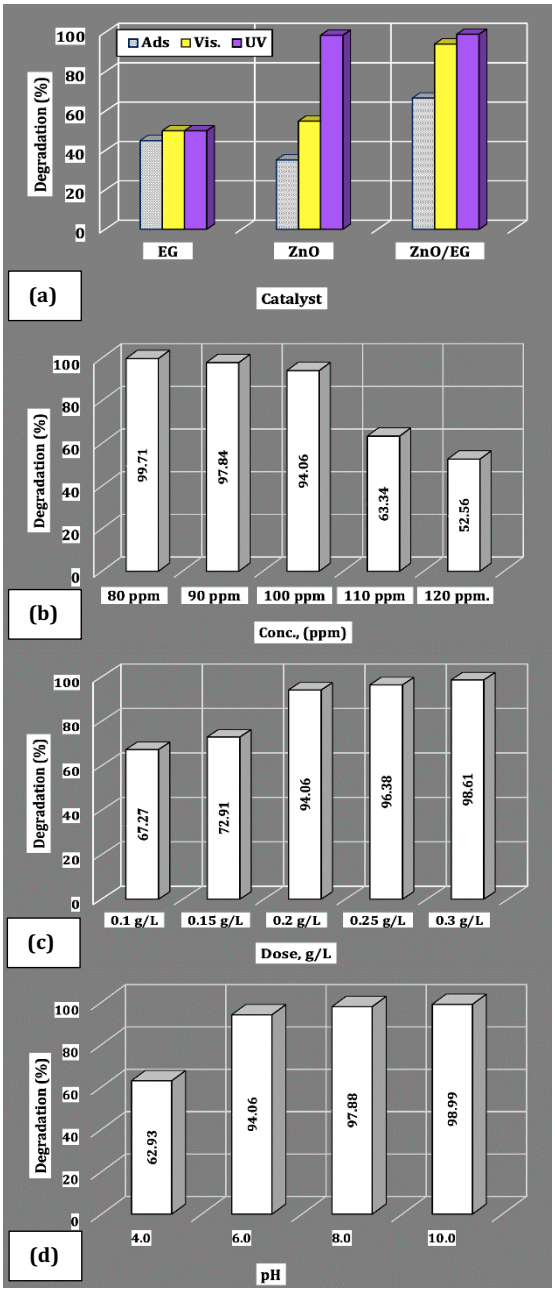

Fig. 7. (a) Effect of the different photocatalysts on the MG adsorption and degradation under both UV and visible light irradiation, (photocatalyst dose = 0.2 g/L, [MG] = 100 ppm, pH 6), (b) effect of the MG concentration (dose = 0.2 g/L, pH 6), (c) effect of the ZnO/EG dose ([MG] = 100 ppm, pH 6) and (d) effect of the solution pH (dose = 0.2 g/L, [MG] = 100 ppm) on the photocatalytic degradation under visible light irradiation.

This significant adsorption performance allows for a greater concentration of MG molecules surrounding the ZnO/EG active sites, accelerating the photodegradation mechanism ahead. Finally, the active species generated (h^+, $^{\bullet}OH$ and $^{\bullet}O_2^-$) react with MG, causing fast photodegradation [46–48].

For ZnO/EG sample, the MG photodegradation was decreased from 99.04 % under UV irradiation to be 94.06 % under visible light irradiation. The extremely intense UV photons compared to the relatively energetic visible photons could be the cause of this minor shift. As the photodegradation process is a chemical reaction that works under light irradiation and follows a pseudo-first-order kinetic model, thus, the photodegradation (%), rate constants (k) and the half-life time ($t_{½}$), Eq. (1) – Eq. (3), are crucial to evaluate the photocatalyst performance, **Table 2**.

$$Ln (C_o/C) = -kt \quad \text{Eq. (1)}$$

$$t_{½} = 0.693/k \quad \text{Eq. (2)}$$

$$Deg (\%) = (C_o - C)/C_o *100 \quad \text{Eq. (3)}$$

Where, C_o and C are the initial and final MG concentrations, respectively.

Table 2

Determination of the degradation (%), rate constant, (k, min^{-1}), half-life time, ($t_{½}$, min), and determination coefficient (R^2), under both UV and visible light irradiation, (photocatalyst dose = 0.2 g/L, [MG] = 100 ppm).

Light Source	Sample	EG	ZnO	ZnO/EG
UV	**Deg (%)**	50.05	98.51	99.04
	k	0.0030	0.0283	0.0247
	$t_{½}$	231.0	24.5	28.1
	R^2	0.982	0.987	0.990
Vis.	**Deg (%)**	50.05	54.91	94.06
	k	0.0030	0.0044	0.0184
	$t_{½}$	231.0	157.5	37.7
	R^2	0.985	0.988	0.992

3.2.1. The effect of different parameters on the ZnO/EG photocatalytic performance

Fig. 7 (b–d) represents the effect of various parameters on the photocatalytic performance of the binary nanocomposite ZnO/EG toward the MG dye photodegradation under visible light irradiation, including initial MG dye concentration, photocatalyst dose, and solution pH. The effect of the initial pollutant concentration on the ZnO/EG photocatalytic performance was studied in the MG dye concentration range (80–120 ppm), **Fig. 7 (b)**, where the other

factors were kept constant. It was found that increasing the dye concentration reduced MG photodegradation, which could be related to a reduction in photons reaching the ZnO/EG surface. Moreover, the optical density of the MG solution is increased by increasing the MG concentration forming an inner filter for the incident light, as well as blocking more positions of the ZnO/EG photocatalyst's accessible sites [49,50].

The effect of the ZnO/EG dose on its photocatalytic performance toward MG dye photodegradation was studied in the range (0.1–0.3 g/L), **Fig. 7 (c)**, where the other factors were kept constant. When the photocatalyst dose was raised in the range of 0.1–0.3 g/L, the MG photodegradation was significantly enhanced due to an increase in the quantity of the available photocatalyst's active sites with constant MG concentration [51].

The wastewater effluents of the textile industry frequently have a wide pH values range. The pH value was discovered to play a significant effect on the properties of wastewater effluents, organic adsorption on adsorbents/photocatalysts, and active species generation. As a result, pH may be one of the most important parameters influencing photodegradation. The adsorption process is influenced by the structure and solubility of the dye, as well as the charge of the adsorbent surface, which is affected by the dye pH, and hence affecting the ionic interaction between the dye and ZnO/EG which strongly affect the photocatalytic degradation [52–54].

Therefore, the effect of the MG solution pH on the photodegradation by ZnO/EG composite was studied in the range (4.0–10.0) and was adjusted by 0.1 M HCl or NaOH, with the other parameters were kept constant. It is generally known that the dye colour was self-fed at pH 10.5 and above. This could be attributed to the formation of new dye species. The most favourable degradation was observed at basic pH 6–10 with 94.06 – 98.99% removal of MG dye, respectively (**Fig. 7 (d)**). At lower pH (pH 4), the number of positively (+) charged surface sites increases more than the number of negatively (-) charged surface sites. Moreover, the –COOH groups of MG were protonated and had a high positive charge density. As a result, as the solution pH decreased, electrostatic repulsion between the (+) charged surface and the (+) charged dye molecule increased, reducing MG adsorption and therefore photodegradation. Furthermore, the adsorption was reduced due to competition between the H^+ ion and the (+) charged dye molecules. At higher pH, the photocatalyst's surface was (-) charged which favoured for adsorption of the (+) charged dye molecules via electrostatic attraction force. Consequently, the MG adsorption on the ZnO/EG photocatalyst and hence the photodegradation increased with increasing the pH values up to pH 10 [55].

3.2.2. Photodegradation Mechanism

Eq. (4)–Eq. (11) express the general photodegradation mechanism of semiconductors regarding the MG dye as a contaminant. Exposure to photons initiates photocatalytic reactions, which result in the creation of photo-induced electrons (e^-) in the valence band (VB), which are then transferred to the conduction band (CB), leaving behind positive holes (h^+) in the VB, Eq. (4). The e^-–h^+ pairs are the main charge carriers responsible for semiconductor activity. The h^+ in the VB could directly (Eq. (5)) or indirectly, Eq. (6), oxidize organic pollutants by forming hydroxyl radicals ($OH^·$), which have high oxidizing power and can degrade most organic dyes efficiently, Eq. (7). The e^- in the CB, on the other hand, can degrade organic pollutants either directly (Eq. (8)) or indirectly, Eq. (9), by the creation of $O^·_2{}^-$, which can directly break down organic pollutants, Eq. (10). As a result, these reactive species e^-, h^+, $O^·_2{}^-$, and $OH^·$ are the main species in the photocatalytic degradation of MG. The emission of heat or photons follows the recombination of e^- and h^+ Eq. (11). Recombination would reduce the development of the reactive species, necessitating a return to the initiation process to create new pairs of e^- and h^+ [5].

$$\text{Semiconductor} + h\upsilon \rightarrow e^-_{CB} + h^+_{VB} \quad \textit{Eq. (4)}$$

$$MG + h^+_{VB} \rightarrow MG^+ \rightarrow \textit{Degraded Products} \quad \text{Eq. (5)}$$

$$H_2O + h^+_{VB} \rightarrow OH^· \quad \text{Eq. (6)}$$

$$MG + OH^· \rightarrow MG^+ \rightarrow \textit{Degraded Products} \quad \text{Eq. (7)}$$

$$MG + e^-_{CB} \rightarrow MG^- \rightarrow \textit{Degraded Products} \quad \text{Eq. (8)}$$

$$O_2 + e^-_{CB} \rightarrow O^·_2{}^- \quad \text{Eq. (9)}$$

$$MG + O^·_2{}^- \rightarrow MG^- \rightarrow \textit{Degraded Products} \quad \text{Eq. (10)}$$

$$e^-_{CB} + h^+_{VB} \rightarrow \text{heat or } h\upsilon \quad \text{Eq. (11)}$$

To understand the MG dye photocatalytic degradation mechanism by ZnO/EG photocatalyst, the role of the active species was determined by the trapping experiments. In this regard, (100 mM) iso-butanol (But), (1 mM) p-benzoquinone (BQ), and (100 mM) ammonium oxalate (AO) were used as target scavengers for hydroxyl ($OH^•$), superoxide ($O^·_2{}^-$), and photo-generated (h^+), respectively [56]. The MG dye was degraded by (94.06 %) in the absence of any scavengers, while this percentage is slightly decreased by (< 6 %) in the presence of iso-butanol and benzoquinone separately, **Fig. 8 (a)**, suggesting the minor role of ($OH^•$) and ($O^·_2{}^-$) radicals for the promotion of the degradation process. However, in the presence of the ammonium oxalate as a scavenger, the activity greatly decreased by (15 %) to be (79.53 %), confirming the major role of the holes (h^+) in the degradation process of MG. Moreover, the improved

photocatalytic efficiency at high pH values and the enhancement in MG photodegradation behaviour when the h^+ is increased, as well as the high reduction in the photodegradation of MG in the existence of the AO, reveal that the holes in the valence band are the most reactive species in photocatalytic processes and that the oxidative degradation pathway is the most common. The same finding is discussed by Moussa et al. [43] they prepared ZnO supported on graphitic carbon nitride; ZnO/gCN; for the photodegradation of dye under visible light irradiation and found that the holes are one of the major reactive species in which the holes in the carbon material are responsible for the dye oxidation. Also, Ao et al. [57] and Feng et al. [58] found that $OH^{\bullet}$ radicals had a minimal effect on the degradation process [2].

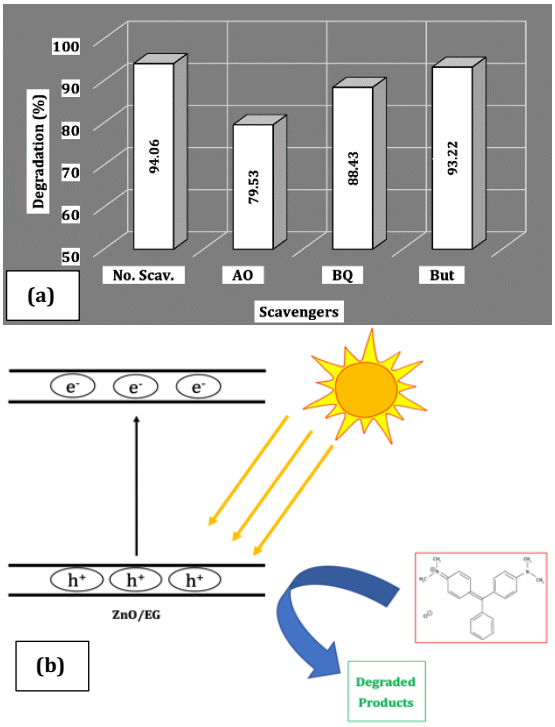

Fig. 8. (a) Effect of the different scavengers on the photodegradation of MG over ZnO/EG photocatalyst under visible light irradiation, (photocatalyst dose = 0.2 g/L, [MG] = 100 ppm, time = 180 min). (b) Pictorial representation of the suggested mechanism.

4. Conclusions

In summary, ZnO NPs were synthesized using *Streptomyces* microbial extract as a reducing and capping agent. The biosynthesized ZnO NPs were supported on the exfoliated graphite by a simple low-cost mixing method. The photocatalytic performance of the prepared samples was studied for MG dye degradation under both UV and visible light irradiation. Structural analysis by XRD proved the existence of hexagonal Wurtzite ZnO nanostructures. The results demonstrate that the supporting of the ZnO on the EG widens the light absorption of the ZnO/EG composite towards the visible light and enhances the charge separation. Moreover, the negative zeta potential of the composite increased, which enhances the MG dye adsorption behaviour. These results together elucidate the outstanding photocatalytic performance of the ZnO/EG composite for the MG dye degradation under visible light irradiation. Almost, 94.06 % photocatalytic efficiency was achieved for MG (MG conc. = 100 ppm, dose = 0.2 g/L). Also, the scavenger's tests clarify that the holes are the major reactive species responsible for the photocatalytic process, confirming that the oxidative degradation pathway is the dominant pathway. Moreover, the photodegradation process was affected by the change in the dye concentration, catalyst dose and pH changes. When the dye concentration increased, the efficiency decreased, while, when the catalyst dose increased, the efficiency increased. Additionally, increasing the pH toward pH 10 enhances the efficiency. These results are promising and compete for photocatalytic degradation under visible light for wastewater treatment applications.

5. Conflicts of interest

There are no conflicts to declare.

6. Funding

No funds, grants, or other support was received.

7. References

[1] R.K. Thines, N.M. Mubarak, S. Nizamuddin, J.N. Sahu, E.C. Abdullah, P. Ganesan, Application potential of carbon nanomaterials in water and wastewater treatment: A review, J. Taiwan Inst. Chem. Eng. 72 (2017) 116–133. https://doi.org/10.1016/j.jtice.2017.01.018.

[2] S. Munyai, Z.N. Tetana, M.M. Mathipa, B. Ntsendwana, N.C. Hintsho-Mbita, Green synthesis of Cadmium Sulphide nanoparticles for the photodegradation of Malachite green dye, Sulfisoxazole and removal of bacteria, Optik (Stuttg). 247 (2021) 167851. https://doi.org/10.1016/j.ijleo.2021.167851.

[3] P. Das, S. Ghosh, R. Ghosh, S. Dam, M. Baskey, Madhuca longifolia plant mediated green synthesis of cupric oxide nanoparticles: A promising environmentally sustainable material for waste water treatment and efficient antibacterial agent, J. Photochem. Photobiol. B Biol. 189 (2018) 66–73. https://doi.org/10.1016/j.jphotobiol.2018.09.023.

[4] C. Prasad, K. Sreenivasulu, S. Gangadhara, P. Venkateswarlu, Bio inspired green synthesis of Ni/Fe_3O_4 magnetic nanoparticles using Moringa

oleifera leaves extract: A magnetically recoverable catalyst for organic dye degradation in aqueous solution, J. Alloys Compd. 700 (2017) 252–258. https://doi.org/10.1016/j.jallcom.2016.12.363.

[5] E.M. Hashem, M.A. Hamza, A.N. El-Shazly, S.A. Abd El-Rahman, E.M. El-Tanany, R.T. Mohamed, N.K. Allam, Novel Z-Scheme/Type-II CdS@ZnO/g-C_3N_4 ternary nanocomposites for the durable photodegradation of organics: Kinetic and mechanistic insights, Chemosphere. 277 (2021) 128730. https://doi.org/10.1016/j.chemosphere.2020.128730.

[6] X. Li, L. Ai, J. Jiang, Nanoscale zerovalent iron decorated on graphene nanosheets for Cr(VI) removal from aqueous solution: Surface corrosion retard induced the enhanced performance, Chem. Eng. J. 288 (2016) 789–797. https://doi.org/10.1016/j.cej.2015.12.022.

[7] S.J. Tshemese, W. Mhike, S.M. Tichapondwa, Adsorption of phenol and chromium (VI) from aqueous solution using exfoliated graphite: Equilibrium, kinetics and thermodynamic studies, Arab. J. Chem. 14 (2021) 103160. https://doi.org/10.1016/j.arabjc.2021.103160.

[8] V.H. Nguyen, L.A. Phan Thi, Q. Van Le, P. Singh, P. Raizada, P. Kajitvichyanukul, Tailored photocatalysts and revealed reaction pathways for photodegradation of polycyclic aromatic hydrocarbons (PAHs) in water, soil and other sources, Chemosphere. 260 (2020) 127529. https://doi.org/10.1016/j.chemosphere.2020.127529.

[9] A. Hsini, Y. Naciri, M. Laabd, M. El Ouardi, Z. Ajmal, R. Lakhmiri, R. Boukherroub, A. Albourine, Synthesis and characterization of arginine-doped polyaniline/walnut shell hybrid composite with superior clean-up ability for chromium (VI) from aqueous media: Equilibrium, reusability and process optimization, J. Mol. Liq. 316 (2020) 113832. https://doi.org/10.1016/j.molliq.2020.113832.

[10] E. Amdeha, Recovery of Nanomaterials from Agricultural and Industrial Wastes for Water Treatment Applications, in: A.S.H. Makhlouf, G.A.M. Ali (Eds.), Waste Recycl. Technol. Nanomater. Manuf., Springer, Cham, 2021: pp. 385–417. https://doi.org/10.1007/978-3-030-68031-2_14.

[11] X. Hu, H. Zhao, Y. Liang, F. Chen, J. Li, R. Chen, Broad-spectrum response NCQDs/$Bi_2O_2CO_3$ heterojunction nanosheets for ciprofloxacin photodegradation: Unraveling the unique roles of NCQDs upon different light irradiation, Chemosphere. 264 (2021) 128434. https://doi.org/10.1016/j.chemosphere.2020.128434.

[12] R.A. El-Salamony, E. Amdeha, A.M. El Shafey, A.M. Al Sabagh, Preparation and characterisation of Ce-doped SiO_2 nano-materials as effective photo-catalyst under visible light, Int. J. Environ. Anal. Chem. (2021). https://doi.org/10.1080/03067319.2020.1865328.

[13] M.A. Hamza, A.N. El-Shazly, S.A. Tolba, N.K. Allam, Novel Bi-based photocatalysts with unprecedented visible light-driven hydrogen production rate: Experimental and DFT insights, Chem. Eng. J. 384 (2020) 123351. https://doi.org/10.1016/j.cej.2019.123351.

[14] H. Agarwal, S. Venkat Kumar, S. Rajeshkumar, A review on green synthesis of zinc oxide nanoparticles – An eco-friendly approach, Resour. Technol. 3 (2017) 406–413. https://doi.org/10.1016/j.reffit.2017.03.002.

[15] S.M. Aydoghmish, S.A. Hassanzadeh-Tabrizi, A. Saffar-Teluri, Facile synthesis and investigation of NiO–ZnO–Ag nanocomposites as efficient photocatalysts for degradation of methylene blue dye, Ceram. Int. 45 (2019) 14934–14942. https://doi.org/10.1016/j.ceramint.2019.04.229.

[16] C. Zhang, P. Li, B. Cao, Fabrication of superhydrophobic-superoleophilic fabrics by an etching and dip-coating two-step method for oil-water separation, Ind. Eng. Chem. Res. 55 (2016) 5030–5035. https://doi.org/10.1021/acs.iecr.6b00206.

[17] B. Hou, H.J. Sun, T.J. Peng, X.Y. Zhang, Y.Z. Ren, Rapid preparation of expanded graphite at low temperature, Xinxing Tan Cailiao/New Carbon Mater. 35 (2020) 262–268. https://doi.org/10.1016/S1872-5805(20)60488-7.

[18] M.N. Carvallho, K.S. Da Silva, D.C.S. Sales, E.M.P.L. Freire, M.A.M. Sobrinho, M.G. Ghislandi, Dye removal from textile industrial effluents by adsorption on exfoliated graphite nanoplatelets: Kinetic and equilibrium studies, Water Sci. Technol. 73 (2016) 2189–2198. https://doi.org/10.2166/wst.2016.073.

[19] T. Van Pham, T. Van Tran, T.D. Nguyen, N.T.H. Tham, P.T.T. Quang, D.T.T. Uyen, N.T.H. Le, D.V.N. Vo, N.T. Thanh, L.G. Bach, Adsorption behavior of Congo red dye from aqueous solutions onto exfoliated graphite as an adsorbent: Kinetic and isotherm studies, Mater. Today Proc. 18 (2019) 4449–4457. https://doi.org/10.1016/j.matpr.2019.07.414.

[20] M.. A. El-Meleigy, M.M. Mohamadein, H.F. Mohamed, M.S. Salem, Morphological, Biochemical and Sequence-Based Identification of Some Selenium Tolerant Actinomycetes, New York Sci. J. 4 (2011) 20–26. http://www.sciencepub.net/newyorkhttp://www.

sciencepub.net/newyork (accessed March 30, 2022).

[21] M. Naseer, U. Aslam, B. Khalid, B. Chen, Green route to synthesize Zinc Oxide Nanoparticles using leaf extracts of Cassia fistula and Melia azadarach and their antibacterial potential, Sci. Rep. 10 (2020). https://doi.org/10.1038/s41598-020-65949-3.

[22] C.W. Chang, Y.H. Kao, P.H. Shen, P.C. Kang, C.Y. Wang, Nanoconfinement of metal oxide MgO and ZnO in zeolitic imidazolate framework ZIF-8 for CO_2 adsorption and regeneration, J. Hazard. Mater. 400 (2020) 122974. https://doi.org/10.1016/j.jhazmat.2020.122974.

[23] P. Zhu, X. Yin, X. Gao, G. Dong, J. Xu, C. Wang, Enhanced photocatalytic NO removal and toxic NO_2 production inhibition over ZIF-8-derived ZnO nanoparticles with controllable amount of oxygen vacancies, Chinese J. Catal. 42 (2020) 175–183. https://doi.org/10.1016/S1872-2067(20)63592-6.

[24] Y. Lin, C. Zhu, G. Alva, G. Fang, Palmitic acid/polyvinyl butyral/expanded graphite composites as form-stable phase change materials for solar thermal energy storage, Appl. Energy. 228 (2018) 1801–1809. https://doi.org/10.1016/j.apenergy.2018.07.068.

[25] C. Dai, C. Gu, B. Liu, Y. Lyu, X. Yao, H. He, J. Fang, G. Zhao, Preparation of low-temperature expandable graphite as a novel steam plugging agent in heavy oil reservoirs, J. Mol. Liq. 293 (2019) 111535. https://doi.org/10.1016/j.molliq.2019.111535.

[26] M. Usha Rani, K. Nanaji, T.N. Rao, A.S. Deshpande, Corn husk derived activated carbon with enhanced electrochemical performance for high-voltage supercapacitors, J. Power Sources. 471 (2020) 228387. https://doi.org/10.1016/j.jpowsour.2020.228387.

[27] S. Ambika, V. Srilekha, Eco-safe chemicothermal conversion of industrial graphite waste to exfoliated graphene and evaluation as engineered adsorbent to remove toxic textile dyes, Environ. Adv. 4 (2021) 100072. https://doi.org/10.1016/j.envadv.2021.100072.

[28] L. Zhao, Q. Yu, M. Li, Y. Zhang, Y. Wang, D. Zhan, S. Jin, Y. Huang, Preparation and thermal properties of low-temperature composite phase-change materials based on a binary eutectic mixture with expanded graphite: Effect of particle size and mass fraction, J. Energy Storage. 40 (2021) 102778. https://doi.org/10.1016/j.est.2021.102778.

[29] P. Wang, H. Sun, T. Peng, The evolution rule of three-dimensional structures of graphite during oxidation, Nano. 10 (2015). https://doi.org/10.1142/S1793292015500149.

[30] M.H. Taha, S.A. Abdel Maksoud, M.M. Ali, A.M.A. El Naggar, A.S. Morshedy, A.A. Elzoghby, Conversion of biomass residual to acid-modified bio-chars for efficient adsorption of organic pollutants from industrial phosphoric acid: an experimental, kinetic and thermodynamic study, Int. J. Environ. Anal. Chem. 99 (2019) 1211–1234. https://doi.org/10.1080/03067319.2019.1618459.

[31] J. Santhoshkumar, S.V. Kumar, S. Rajeshkumar, Synthesis of zinc oxide nanoparticles using plant leaf extract against urinary tract infection pathogen, Resour. Technol. 3 (2017) 459–465. https://doi.org/10.1016/j.reffit.2017.05.001.

[32] S. Wang, C. Wang, X. Ji, Towards understanding the salt-intercalation exfoliation of graphite into graphene, RSC Adv. 7 (2017) 52252–52260. https://doi.org/10.1039/c7ra07489a.

[33] D. Khalili, Graphene oxide: A promising carbocatalyst for the regioselective thiocyanation of aromatic amines, phenols, anisols and enolizable ketones by hydrogen peroxide/KSCN in water, New J. Chem. 40 (2016) 2547–2553. https://doi.org/10.1039/c5nj02314a.

[34] R.S. Prakasham, B.S. Kumar, Y.S. Kumar, K.P. Kumar, Production and Characterization of Protein Encapsulated Silver Nanoparticles by Marine Isolate Streptomyces parvulus SSNP11, Indian J. Microbiol. 54 (2014) 329–336. https://doi.org/10.1007/s12088-014-0452-1.

[35] L.H.D.S.. Lakhsmi. S.Y.S., Isolation, Screening, Identification, Characterization and Applications of Green Synthesized Silver Nanoparticle From Marine Actinomycetes-Streptomyces Althioticus, World J. Pharm. Res. 4 (2015) 1592–1611.

[36] J. Santhoshkumar, S.V. Kumar, S. Rajeshkumar, Synthesis of zinc oxide nanoparticles using plant leaf extract against urinary tract infection pathogen, Resour. Technol. 3 (2017) 459–465. https://doi.org/10.1016/j.reffit.2017.05.001.

[37] H.M. Abd-Elnaby, G.M. Abo-Elala, U.M. Abdel-Raouf, M.M. Hamed, Antibacterial and anticancer activity of extracellular synthesized silver nanoparticles from marine Streptomyces rochei MHM13, Egypt. J. Aquat. Res. 42 (2016) 301–312. https://doi.org/10.1016/j.ejar.2016.05.004.

[38] K. Wang, T. Yan, Y.M. Zhao, G.D. Li, W.G. Pan, Preparation and thermal properties of palmitic acid @ZnO/Expanded graphite composite phase change material for heat storage, Energy. 242 (2022) 122972. https://doi.org/10.1016/j.energy.2021.122972.

[39] N. Aziz, T. Fatma, A. Varma, R. Prasad, Biogenic Synthesis of Silver Nanoparticles Using Scenedesmus abundans and Evaluation of Their Antibacterial Activity , J. Nanoparticles. 2014 (2014) 1–6. https://doi.org/10.1155/2014/689419.

[40] A.A. Mohamed, A. Fouda, M.A. Abdel-Rahman, S.E.D. Hassan, M.S. El-Gamal, S.S. Salem, T.I. Shaheen, Fungal strain impacts the shape, bioactivity and multifunctional properties of green synthesized zinc oxide nanoparticles, Biocatal. Agric. Biotechnol. 19 (2019) 101103. https://doi.org/10.1016/j.bcab.2019.101103.

[41] R.A. El-Salamony, E. Amdeha, N.A. Badawy, S.A. Ghoneim, A.M. Al-Sabagh, Visible light sensitive activated carbon-metal oxide (TiO_2, WO_3, NiO, and SnO) nano-catalysts for photo-degradation of methylene blue: a comparative study, Toxicol. Environ. Chem. 100 (2018) 143–156. https://doi.org/10.1080/02772248.2018.1497634.

[42] S.B. Atla, W.R. Lin, T.C. Chien, M.J. Tseng, J.C. Shu, C.C. Chen, C.Y. Chen, Fabrication of Fe_3O_4/ZnO magnetite core shell and its application in photocatalysis using sunlight, Mater. Chem. Phys. 216 (2018) 380–386. https://doi.org/10.1016/j.matchemphys.2018.06.020.

[43] H. Moussa, B. Chouchene, T. Gries, L. Balan, K. Mozet, G. Medjahdi, R. Schneider, Growth of ZnO Nanorods on Graphitic Carbon Nitride gCN Sheets for the Preparation of Photocatalysts with High Visible-Light Activity, ChemCatChem. 10 (2018) 4987–4997. https://doi.org/10.1002/cctc.201801206.

[44] X. Gao, P.G. Ren, J. Wang, F. Ren, Z. Dai, Y.L. Jin, Fabrication of visible-light responsive TiO_2@C photocatalyst with an ultra-thin carbon layer to efficiently degrade organic pollutants, Appl. Surf. Sci. 532 (2020) 147482. https://doi.org/10.1016/j.apsusc.2020.147482.

[45] X. Chen, M. Zhang, H. Qin, J. Zhou, Q. Shen, K. Wang, W. Chen, M. Liu, N. Li, Synergy effect between adsorption and heterogeneous photo-Fenton-like catalysis on $LaFeO_3$/lignin-biochar composites for high efficiency degradation of ofloxacin under visible light, Sep. Purif. Technol. 280 (2022) 119751. https://doi.org/10.1016/j.seppur.2021.119751.

[46] T.T.N. Phan, A.N. Nikoloski, P.A. Bahri, D. Li, Adsorption and photo-Fenton catalytic degradation of organic dyes over crystalline $LaFeO_3$-doped porous silica, RSC Adv. 8 (2018) 36181–36190. https://doi.org/10.1039/c8ra07073c.

[47] B. Abramovic, V. Despotovic, D. Šojic, N. Fincur, Mechanism of clomazone photocatalytic degradation: Hydroxyl radical, electron and hole scavengers, React. Kinet. Mech. Catal. 115 (2015) 67–79. https://doi.org/10.1007/s11144-014-0814-z.

[48] M. Cheng, G. Zeng, D. Huang, C. Lai, P. Xu, C. Zhang, Y. Liu, J. Wan, X. Gong, Y. Zhu, Degradation of atrazine by a novel Fenton-like process and assessment the influence on the treated soil, J. Hazard. Mater. 312 (2016) 184–191. https://doi.org/10.1016/j.jhazmat.2016.03.033.

[49] M.A. Ahmed, Z.M. Abou-Gamra, H.A.A. Medien, M.A. Hamza, Effect of porphyrin on photocatalytic activity of TiO_2 nanoparticles toward Rhodamine B photodegradation, J. Photochem. Photobiol. B Biol. 176 (2017) 25–35. https://doi.org/10.1016/j.jphotobiol.2017.09.016.

[50] Y. Naciri, H. Ait Ahsaine, A. Chennah, A. Amedlous, A. Taoufyq, B. Bakiz, M. Ezahri, S. Villain, A. Benlhachemi, Facile synthesis, characterization and photocatalytic performance of $Zn_3(PO_4)_2$ platelets toward photodegradation of Rhodamine B dye, J. Environ. Chem. Eng. 6 (2018) 1840–1847. https://doi.org/10.1016/j.jece.2018.02.009.

[51] Z.M. Abou-Gamra, M.A. Ahmed, M.A. Hamza, Investigation of commercial $PbCrO_4$/TiO_2 for photodegradation of rhodamine B in aqueous solution by visible light, Nanotechnol. Environ. Eng. 2 (2017) 1–10. https://doi.org/10.1007/s41204-017-0024-9.

[52] N. Sykam, N.D. Jayram, G.M. Rao, Highly efficient removal of toxic organic dyes, chemical solvents and oils by mesoporous exfoliated graphite: Synthesis and mechanism, J. Water Process Eng. 25 (2018) 128–137. https://doi.org/10.1016/j.jwpe.2018.05.013.

[53] I. Shittu, A. Achazhiyath Edathil, A. Alsaeedi, S. Al-Asheh, K. Polychronopoulou, F. Banat, Development of novel surfactant functionalized porous graphitic carbon as an efficient adsorbent for the removal of methylene blue dye from aqueous solutions, J. Water Process Eng. 28 (2019) 69–81. https://doi.org/10.1016/j.jwpe.2019.01.001.

[54] Z. Hu, L. Cai, J. Liang, X. Guo, W. Li, Z. Huang, Green synthesis of expanded graphite/layered double hydroxides nanocomposites and their application in adsorption removal of Cr(VI) from aqueous solution, J. Clean. Prod. 209 (2019) 1216–1227. https://doi.org/10.1016/j.jclepro.2018.10.295.

[55] A.S. Sartape, A.M. Mandhare, V. V. Jadhav, P.D. Raut, M.A. Anuse, S.S. Kolekar, Removal of malachite green dye from aqueous solution with adsorption technique using Limonia

acidissima (wood apple) shell as low cost adsorbent, Arab. J. Chem. 10 (2017) S3229–S3238. https://doi.org/10.1016/j.arabjc.2013.12.019.

[56] E. Amdeha, R.S. Mohamed, A.S. Dhmees, Sonochemical assisted preparation of ZnS–ZnO/MCM-41 based on blast furnace slag and electric arc furnace dust for Cr (VI) photoreduction, Ceram. Int. 47 (2021) 23014–23027. https://doi.org/10.1016/j.ceramint.2021.05.015.

[57] Y. Ao, L. Xu, P. Wang, C. Wang, J. Hou, J. Qian, Preparation of CdS nanoparticle loaded flower-like $Bi_2O_2CO_3$ heterojunction photocatalysts with enhanced visible light photocatalytic activity, Dalt. Trans. 44 (2015) 11321–11330. https://doi.org/10.1039/c5dt01168j.

[58] Y. Feng, X. Yan, C. Liu, Y. Hong, L. Zhu, M. Zhou, W. Shi, Hydrothermal synthesis of CdS/Bi_2 MoO_6 heterojunction photocatalysts with excellent visible-light-driven photocatalytic performance, Appl. Surf. Sci. 353 (2015) 87–94. https://doi.org/10.1016/j.apsusc.2015.06.061.